

Holographic QCD Running Coupling for Heavy Quarks in Strong Magnetic Field

Irina Ya. Aref'eva^a, Ali Hajilou^a, Alexander Nikolaev^a, Pavel Slepov^a

^a*Steklov Mathematical Institute, Russian Academy of Sciences,*

Gubkina str. 8, 119991, Moscow, Russia

E-mail: arefeva@mi-ras.ru, hajilou@mi-ras.ru, nikolaev@mi-ras.ru,
slepov@mi-ras.ru

ABSTRACT: We extend our previous work [1], which investigated the influence of a magnetic field on the running coupling constant in a bottom-up holographic light-quark model, to the case of a heavy-quark model. To achieve this, we employ a magnetized Einstein-Maxwell-dilaton background that captures the essential features of heavy quark dynamics. Similar to the light-quark model, the running coupling α for heavy quarks decreases in the presence of a strong external magnetic field at fixed temperature and chemical potential. The key distinction between the light and heavy quark models lies in the locations of their respective phase transitions. However, near the 1st order phase transitions, the behavior of α is analogous for both cases: α exhibits jumps that depend on temperature, chemical potential, and magnetic field strength.

KEYWORDS: AdS/QCD, holography, running coupling constant, heavy quarks, magnetic field

Contents

1	Introduction	2
2	Gravitational Setup for Heavy-Quarks Model	3
3	Running Coupling in a Magnetized Background	8
4	Conclusion	12

1 Introduction

The primary objective of this work is to extend the analysis of our recent study [1] (hereafter referred to as I), which explored the impact of magnetic fields on the running coupling constant in a bottom-up holographic model for light quarks, to the case of heavy-quark systems. The motivation for this study aligns with that of I, and we direct readers to the Introduction of I for a detailed discussion of the broader context. Both this work and I build upon our earlier research into holographic calculations of the running coupling in isotropic quantum chromodynamics (QCD) [2].

As emphasized in I, the energy-dependent running coupling constant in QCD remains a cornerstone of high-energy physics, with experimental determinations spanning a wide range of energies [3] and primarily in low-density regimes (i.e., low baryon chemical potential). To elucidate the interplay between QCD's phase structure and the running coupling under external magnetic fields, a regime of direct relevance to heavy-ion collision experiments and astrophysical phenomena, a robust theoretical understanding of nonperturbative QCD dynamics at finite chemical potential, strong magnetic fields, and varying quark masses is essential. Holographic approaches [4–7], as demonstrated extensively in the literature, provide a powerful framework for probing these nonperturbative regimes. In this study, we focus on the distinctive features of heavy-quark holographic models, contrasting them with their light-quark counterparts to highlight mass-dependent effects in magnetized environments.

The structure of this paper is organized as follows. In Sect. 2, we introduce the 5-dimensional fully anisotropic holographic models in the presence of a non-zero magnetic field for the heavy-quarks model. Sect. 3, encompasses our results on the study of the effect of the magnetic field on the running coupling constant in the heavy-quarks model. In Sect. 4, we summarize our numerical results obtained for heavy-quarks model by comparing them with the light-quarks model as well as figure out perspectives to extend our results for future research.

2 Gravitational Setup for Heavy-Quarks Model

We take the 5-dimensional Einstein-two Maxwell-dilaton (EMd) system with the action in the Einstein frame, given by equation (I.2.1) (hereafter we indicate references to equations from I as (I.xx), where xx is the equation number in I). We search for solutions of the corresponding equations of motion (EOMs) in the form (I.2.2) - (I.2.4). The equations of motions have the same form (I.2.6)-(I.2.11). Recall that all functions depend on the holograph coordinate z .

The light and heavy quark models are distinguished by the scalar factor $\mathcal{A}(z)$, defined by the warp factor (I.2.4) in the metric (I.2.3). For the "heavy-quark" model a simple choice of the scale factor is $\mathcal{A}(z) = -\mathbf{c} z^2/4$ [8, 9]. The magnetic field has been incorporated for this model with a simple scalar factor in [10, 11]. Here for the heavy-quark model we consider an extended scale factor [12]:

$$\mathcal{A}(z) = -\mathbf{c} z^2/4 - (p - c_B q_B) z^4, \quad (2.1)$$

where $\mathbf{c} = 4R_{gg}/3$, $R_{gg} = 1.16 \text{ GeV}^2$, and $p = 0.273 \text{ GeV}^4$ that can be fixed with the lattice and experimental data for zero magnetic field, i.e. for the case $c_B = 0$ considered in [13]. The main motivation for the choice (2.1) is the effect of the magnetic catalysis.

The boundary conditions for equations (I.2.2) - (I.2.4) have the form (I.2.12)-(I.2.14). The boundary conditions with $z_0 = 0$ has been used in [13], and [9] discusses with $z_0 = z_h$. For our purposes, the choice of the z_0 as a function of z_h will be discussed below.

To investigate the thermodynamics and in particular the free energy of the model, we need to evaluate the blackening function. Solving the EOM (I.2.8) one can obtain the blackening function $g(z)$ as

$$g(z) = e^{c_B z^2} \left[1 - \frac{\tilde{I}_1(z)}{\tilde{I}_1(z_h)} + \frac{\mu^2 (2R_{gg} + c_B (q_B - 1)) \tilde{I}_2(z)}{L^2 \left(1 - e^{(2R_{gg} + c_B (q_B - 1)) \frac{z_h^2}{2}} \right)^2} \left(1 - \frac{\tilde{I}_1(z)}{\tilde{I}_1(z_h)} \frac{\tilde{I}_2(z_h)}{\tilde{I}_2(z)} \right) \right], \quad (2.2)$$

$$\tilde{I}_1(z) = \int_0^z e^{(2R_{gg} - 3c_B) \frac{\xi^2}{2} + 3(p - c_B q_B) \xi^4} \xi^{1 + \frac{2}{\nu}} d\xi, \quad (2.3)$$

$$\tilde{I}_2(z) = \int_0^z e^{(2R_{gg} + c_B (\frac{q_B}{2} - 2)) \xi^2 + 3(p - c_B q_B) \xi^4} \xi^{1 + \frac{2}{\nu}} d\xi. \quad (2.4)$$

Then, considering the metric in (I.2.3) and utilizing the extended scale factor (2.1), the temperature and the entropy for the heavy-quark model are given by

$$\begin{aligned}
T &= \left. \frac{|g'|}{4\pi} \right|_{z=z_h} = \left| -\frac{e^{(2R_{gg}-c_B)\frac{z_h^2}{2}+3(p-c_B q_B)z_h^4} z_h^{1+\frac{2}{\nu}}}{4\pi \tilde{I}_1(z_h)} \times \right. \\
&\times \left. \left[1 - \frac{\mu^2(2R_{gg} + c_B(q_B - 1)) \left(e^{(2R_{gg}+c_B(q_B-1))\frac{z_h^2}{2}} \tilde{I}_1(z_h) - \tilde{I}_2(z_h) \right)}{L^2 \left(1 - e^{(2R_{gg}+c_B(q_B-1))\frac{z_h^2}{2}} \right)^2} \right] \right|, \quad (2.5) \\
s &= \frac{1}{4} \left(\frac{L}{z_h} \right)^{1+\frac{2}{\nu}} e^{-(2R_{gg}-c_B)\frac{z_h^2}{2}-3(p-c_B q_B)z_h^4},
\end{aligned}$$

where we fixed $G_5 = 1$ in the entropy formula. Let us set AdS radius $L = 1$. Calculating the free energy

$$F = - \int s dT = \int_{z_h}^{\infty} s T' dz, \quad (2.6)$$

leads to obtain the phase diagrams for the heavy-quark model. Note that in (2.6) the "T'" is " $\frac{dT}{dz}$ " and we normalized the free energy considering $z_h \rightarrow \infty$ when we have the thermal-AdS background.

The phase diagram (the 1st order phase transition location) for the heavy-quark model in the (μ, T) -plane, considering the isotropic case with $c_B = 0$ and magnetized anisotropic cases with different c_B is shown in Fig. 1A. In this figure, the magenta stars indicate the corresponding critical end points (CEPs) for $c_B = 0$ and $c_B = -0.5$ GeV². Increasing the absolute value of the magnetic field parameter c_B , the length of the phase transition curves in the (μ, T) -plane increases up to $c_B = -0.5$ GeV² and then decreases. The critical transition temperature T_c (the 1st order phase transition temperature) at zero chemical potential, $\mu = 0$, as a function of the magnetic field parameter c_B is depicted in Fig. 1B. This figure shows that T_c increases with increasing absolute value of the magnetic field parameter c_B and confirms the magnetic catalysis phenomenon for the heavy-quark model.

The energy scale E of the boundary field theory corresponds to the prefactor of the metric (I.2.3) [14] (for more details see refs. in I). In other words, the energy scale E (GeV) as a function of the holographic coordinate z (GeV⁻¹) for heavy-quark model is given by

$$E = \frac{\sqrt{\mathbf{b}(z)}}{z} = \frac{e^{-\mathbf{c}z^2/4-(p-c_B q_B)z^4}}{z}, \quad (2.7)$$

where the parameters \mathbf{c} and p have already been introduced in (2.1). The energy scale $E(z)$ is shown in Fig. 2A and zoom in of the left panel is shown in Fig. 2B for different values of the magnetic field parameter c_B .

Fig. 2B illustrates that the energy scale E in the boundary field theory depends not only on the holographic coordinate z but also on the magnetic field parameter

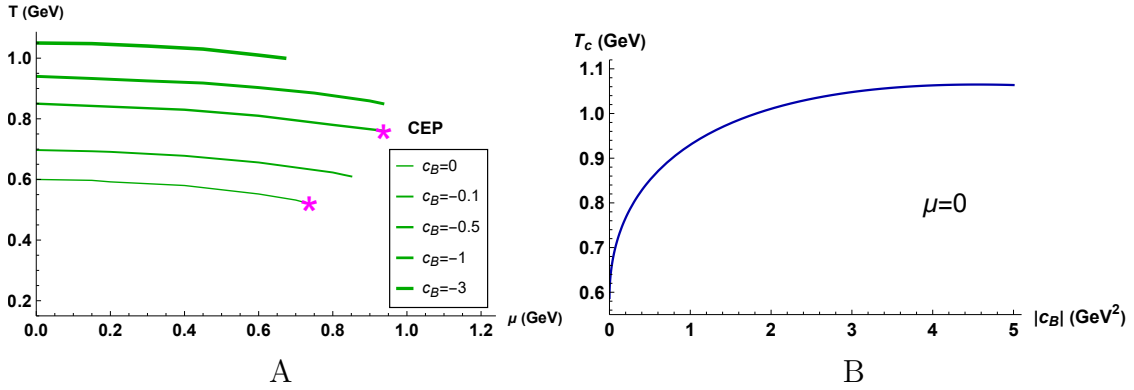


Figure 1. A) Phase diagram of the heavy-quark model in the (μ, T) -plane. The isotropic case is shown with $c_B = 0$ and magnetized anisotropic cases are denoted with different c_B . The magenta stars indicate the CEPs. B) The critical transition temperature at zero chemical potential, $\mu = 0$, as a function of the magnetic field parameter c_B . We set $q_B = 8$.

c_B . Specifically, as the absolute value of c_B increases, the energy scale E decreases more rapidly with respect to z . For a fixed value of z on the gravity side, a larger c_B corresponds to a lower energy scale E on the gauge theory side.

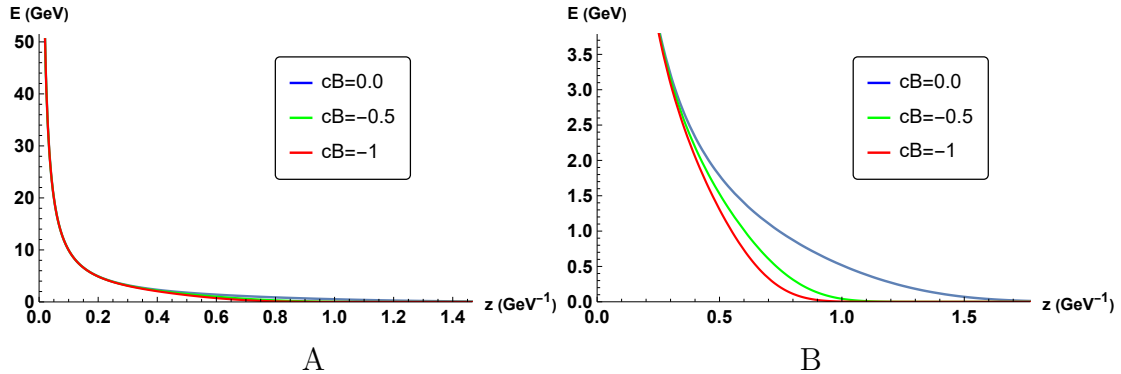


Figure 2. A) Energy scale E (GeV) in the boundary field theory of the heavy-quark model as a function of the holographic coordinate z (GeV⁻¹), corresponding to the warp factor $\mathfrak{b}(z)$ for different values of c_B . B) zoom in of the left panel. We set $q_B = 5$; $[c_B] = \text{GeV}^2$.

2D plots in the (μ, z_h) -plane are shown for $c_B = 0$ in Fig. 3 (top panel), while Fig. 3 (bottom panel) displays the corresponding plots for $c_B = -0.5 \text{ GeV}^2$. The magenta curves represent 1st order phase transitions, consisting of dark and light branches. Fixed temperatures are indicated by brown and blue contours, with $T = 0$ represented by dark red contours. The dark and light branches of the magenta curve are connected at the critical endpoint (CEP), whose coordinates (μ_c, T_c) depend on the magnetic field parameter c_B . Based on Fig. 1, the CEP in Fig. 3B is located at $(\mu_c, T_c) = (0.94, 0.76)$.

The region above the dark branch of the magenta curve and below the light branch corresponds to domains of stable black hole solutions, which represent physical domains. In contrast, the region between the light and dark magenta branches corresponds to a nonphysical domain or unstable solutions. The area between the dark magenta line and the dark red line predominantly represents the hadronic phase, while the region just below the light magenta line corresponds to the quarkyonic phase. For low z_h , the quarkyonic phase transitions into the quark-gluon plasma (QGP) phase (see Fig. 15 of [2] for a more detailed illustration).

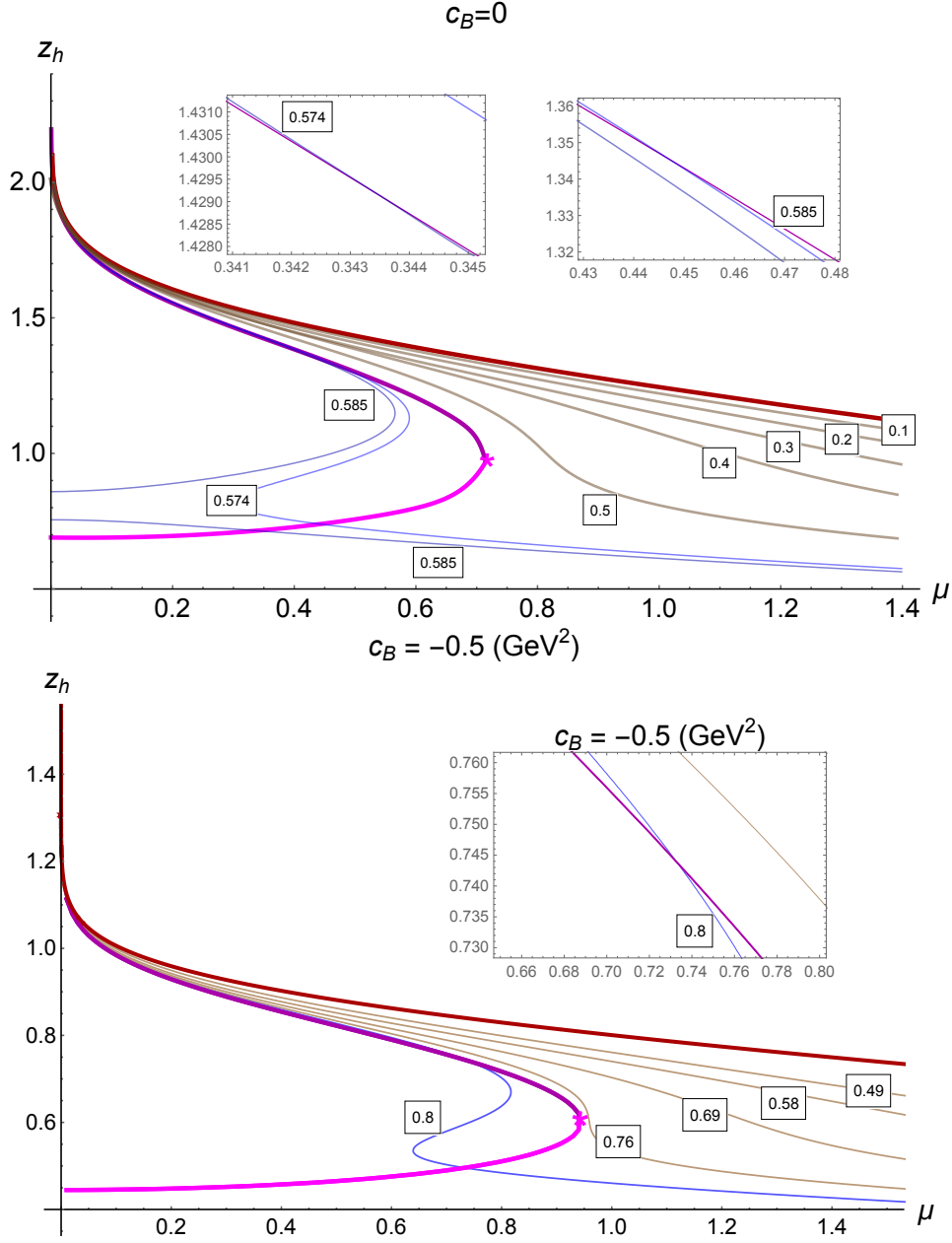


Figure 3. 2D plots in the (μ, z_h) -plane for $c_B = 0$ (top panel) and $c_B = -0.5 \text{ GeV}^2$ (bottom panel). 1st order phase transition lines are shown as magenta curves, with CEPS marked by magenta stars. The domain between magenta lines indicate the unstable domains. Fixed-temperature contours are displayed in brown when they do not intersect the 1st order phase transition lines and in blue where they cross the 1st order transitions. Corresponding temperatures T (in GeV) are annotated in white boxes. The $T = 0$ contours are highlighted in dark red. Zoomed regions in the top panel illustrate intersections between the blue contours and the 1st order transition line. We set $q_B = 5$; $[\mu] = [z_h]^{-1} = \text{GeV}$.

3 Running Coupling in a Magnetized Background

In the holographic approach, the running coupling α as a function of holographic coordinate z , i.e. $\alpha(z)$ is defined in terms of the dilaton field $\varphi(z)$ [15–17].

$$\alpha(z) = e^{\varphi(z)}. \quad (3.1)$$

To obtain the EOM of the dilaton field, we need to solve the system of EOMs (I.2.6) - (I.2.11) contain six equations, although Equ. (I.2.6) is the consequence of other equations and then we have just five independent EOMs. Solving the EOMs (I.2.6) - (I.2.11) needed to fix the form of the scale factor (2.1) and gauge coupling function f_1 [12]. We can consider the following gauge coupling function f_1 for the “heavy-quark” model including magnetic catalysis

$$f_1 = e^{-\left(\frac{2}{3}R_{gg} + \frac{c_B q_B}{2}\right)z^2 + (p - c_B q_B)z^4} \quad (3.2)$$

To obtain the solution for the dilaton field we need to solve EOM (I.2.9) with the the scale factor (2.1). We obtain the following expression

$$\varphi(z) = \int_{z_0}^z \frac{d\xi}{\xi} \left[-4 + \frac{2}{3} \left(6 + 3(-c_B + 6R_{gg})\xi^2 + (-3c_B(c_B + 60q_3) + 4(45p + R_{gg}^2))\xi^4 + 48R_{gg}(p - c_B q_3)\xi^6 + 144(p - c_B q_3)^2 \xi^8 \right) \right]^{\frac{1}{2}}, \quad (3.3)$$

where z_0 is fixed from the boundary condition for the dilaton field defined below.

Note that the dilaton field has a crucial role in defining the holographic running coupling. In addition, the dilaton field $\varphi(z)$ needs to apply a boundary condition to be determined. Therefore, utilizing different boundary conditions lead to different physical results. The boundary condition can be chosen in the following form:

$$\varphi_{z_0}(z) \Big|_{z=z_0} = 0. \quad (3.4)$$

where z_0 is an arbitrary holographic coordinate. The particular form of the boundary condition that corresponds to $z_0 = 0$ is

$$\varphi_0(z) \Big|_{z=0} = 0. \quad (3.5)$$

Considering the modified boundary condition $z_0 = \mathfrak{z}(z_h)$, the running coupling is given by:

$$\alpha_{\mathfrak{z}}(z; T, \mu) = e^{\varphi_0(z) - \varphi_0(\mathfrak{z}(z_h))}. \quad (3.6)$$

See more details about the running coupling definition in [1, 2]. The physical boundary condition for the dilaton field that we consider to study the heavy-quark model [2] is given by

$$z_0 = \mathfrak{z}(z_h) = \exp\left(-\frac{z_h}{4}\right) + 0.1, \quad (3.7)$$

where the dilaton field gets zero at $z = z_0$, as promised in (3.4). Note that the physical boundary condition in (3.7), that was utilized to study the beta-function and renormalization group flow in [18], was derived by investigating the behavior of the QCD string tension as a function of the temperature at zero chemical potential for the isotropic case. For more details see [2]. In spite of the fact that lattice results are not available for the anisotropic case, i.e. $c_B \neq 0$, the physical boundary condition (3.7) is still used in this research.

It is important to note that in studying the behavior of the running coupling constant at different energy scales E , and different magnetic field parameters c_B , we need to respect the physical domains of the model in Fig. 3. The physical domains in (μ, z_h) -plane for nonzero chemical potential are determined by the sizes of the black hole horizons z_h , corresponding to the 1st order phase transition between small and large black holes, denoted by the magenta lines.

In Fig. 4, density plots with contours for the logarithm of the running coupling $\log \alpha_3(E; \mu, T)$ for the heavy-quark model at $c_B = 0$ considering different energy scales $E = \{2.032, 3.212, 6.608\}$ (GeV) in the boundary field theory. Each panel is depicted at a fixed value of energy E -coordinate, which is represented on top of them. The maximum possible temperature values at the corresponding energy scale E are denoted by the red lines in the first two graphs, which arise due to respect the physical condition, i.e. $z \leq z_h$. The fixed values of energy scales in Fig. 4 correspond to holographic coordinates $z = \{0.436, 0.295, 0.150\}$ (GeV^{-1}) represented in Fig. 2. Different but fixed values of $\log \alpha_3$, correspond to different contours in each panel are shown with associated values in the rectangles. By Fig. 4 it is clear that as the energy scale increases, the contours corresponding to the fixed values of the running coupling shift to lower values of the temperature. Therefore, increasing the temperature, the running coupling decreases monotonically, indicating that for a fixed given temperature, the running coupling decreases as the energy scale increases.

In Fig. 5, density plots with contours for $\log \alpha_3(E; \mu, T)$ are depicted such as Fig. 4, but considering $c_B = -0.5 \text{ GeV}^2$. The fixed values of energy scales in Fig. 5 correspond to holographic coordinates $z = \{0.421, 0.294, 0.150\}$ (GeV^{-1}) represented in Fig. 2. Here, the z values are different from $c_B = 0$ because the energy scale E for some domain of energy depends on the magnetic field parameter c_B as well.

The running coupling constant α , as shown in Figs. 4 and 5 shows minimal dependence on the temperature in the hadronic phase for both isotropic ($c_B = 0$) and anisotropic ($c_B = -0.5 \text{ GeV}^2$) cases. However, the running coupling α shows

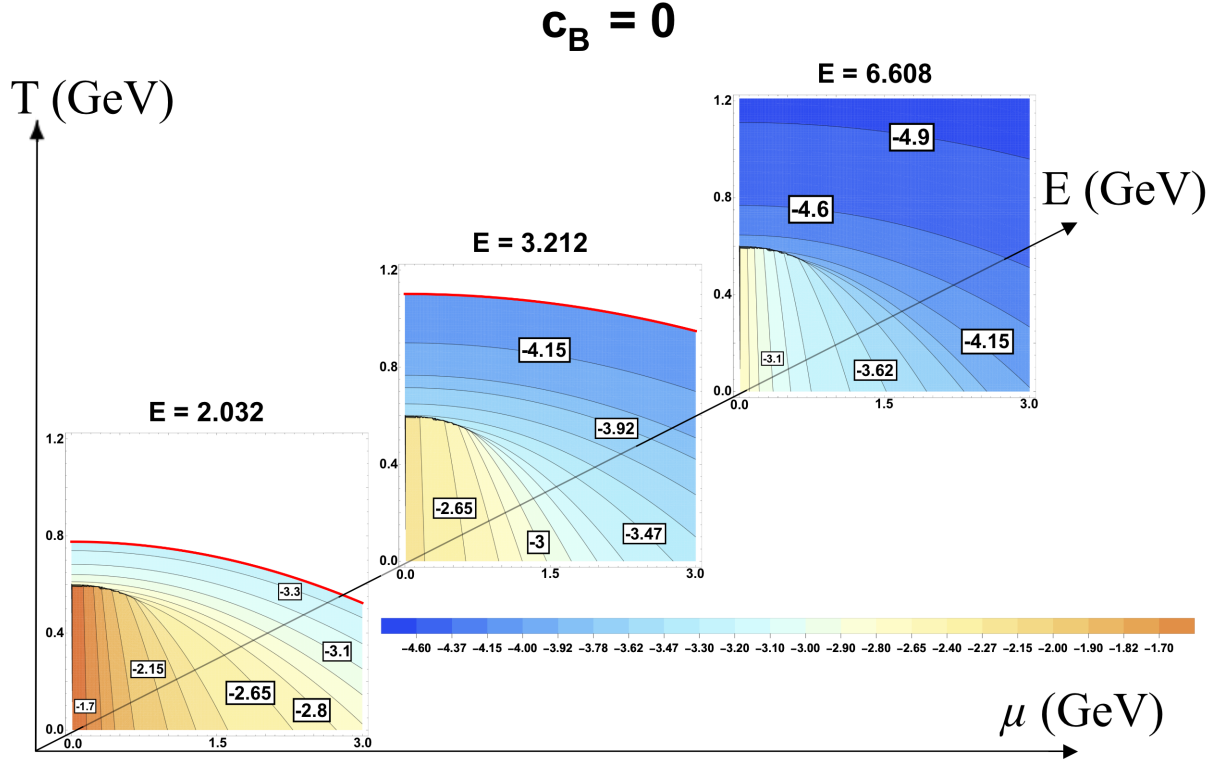


Figure 4. Density plots with contours for $\log \alpha_3(E; \mu, T)$ at different energy scales $E = \{2.032, 3.212, 6.608\}$ (GeV) for $c_B = 0$. All values of E on the top of each panel show fixed value of energy E -coordinate. The red lines in the first two graphs on the left indicate the maximum possible temperature values at the corresponding energy scale E .

significant dependence on the temperature and chemical potential in the QGP phase for both isotropic ($c_B = 0$) and anisotropic ($c_B = -0.5 \text{ GeV}^2$) cases.

The comparison of Fig. 4 ($c_B = 0$) and Fig. 5 ($c_B = -0.5 \text{ GeV}^2$) describes that at fixed values of the parameters of the model ($E; \mu; T$) the strength of the running coupling decreases in the presence of the magnetic field.

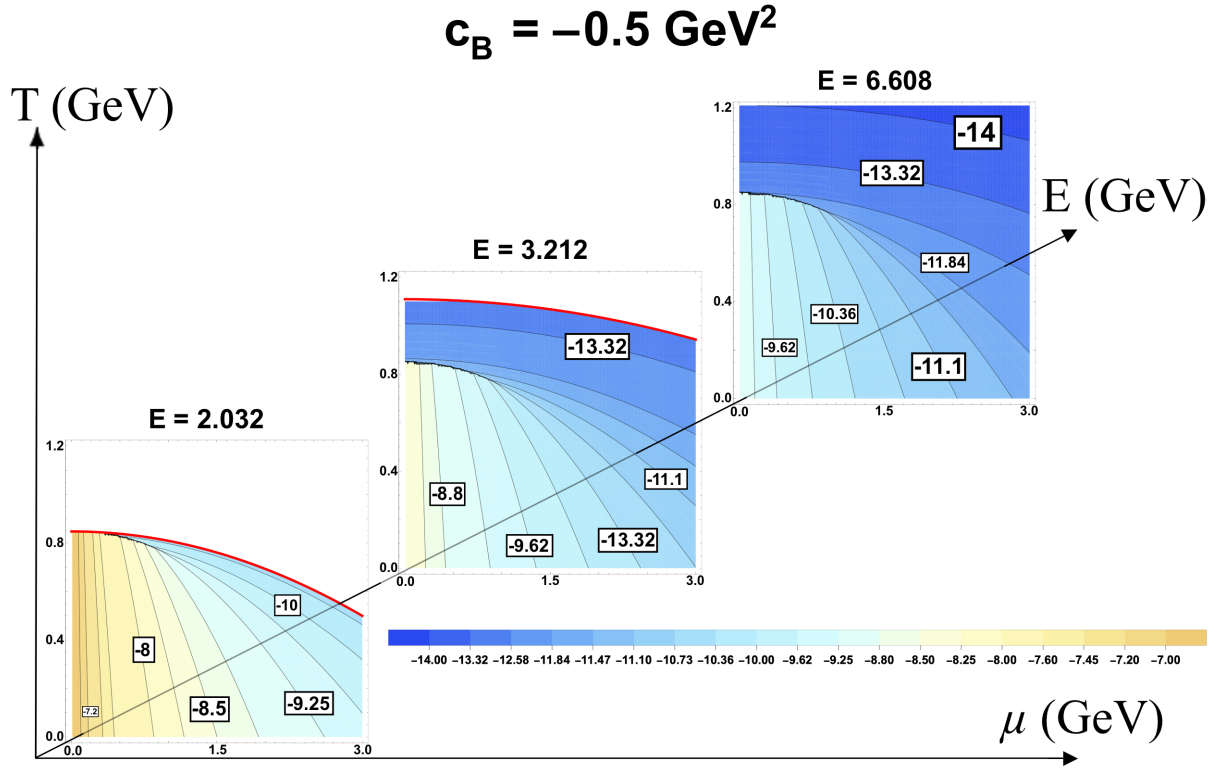


Figure 5. Density plots with contours for $\log \alpha_3(E; \mu, T)$ at different energy scales $E = \{2.032, 3.212, 6.608\}$ (GeV) are shown for $c_B = -0.5 \text{ GeV}^2$. All values of E on the top of each panel show fixed value of energy E -coordinate. These plots illustrate the variation of the running coupling constant across different energy scales, chemical potentials, and temperatures in the presence of a magnetic field. We set $q_B = 5$.

4 Conclusion

In this paper, a companion to our earlier work I, we investigate the behavior of the running coupling constant in an anisotropic holographic model under a strong magnetic field for the heavy-quark case [2]. This complements the analysis in paper I, which focused on the light-quark regime. Both models are constructed using the Einstein-dilaton-two-Maxwell action and incorporate a 5-dimensional metric with a warp factor, extending earlier isotropic frameworks—specifically, the heavy-quark model from [8–13, 19, 20] and the light-quark model in [21–23].

The model of heavy quarks in an external magnetic field has both similarities and significant differences with the model of light quarks

- A key distinction lies in the response to the magnetic field: the heavy-quark model exhibits magnetic catalysis, whereas the light-quark model demonstrates inverse magnetic catalysis. This contrast highlights the interplay between magnetic field strength and quark mass in shaping the phase structure of these holographic models.
- The distinct positions of the 1st order phase transition lines in the two models lead to contrasting behaviors in the discontinuity of α across the 1st order phase transition:
 - For the light-quark model, the jump in α increases with increasing μ .
 - For the heavy-quark model, the jump decreases with increasing μ .

This implies that the CEP is approached by moving along the phase transition line toward higher μ in the heavy-quark model, but toward lower μ in the light-quark model.

For both isotropic ($c_B = 0$) and anisotropic ($c_B = -0.5 \text{ GeV}^2$):

- For light-quark model, in the hadronic phase, α shows minimal variation with changes in μ .
- For heavy-quark model, in the hadronic phase, α shows minimal variation with changes in T .

But there are also some similarities. Namely, the heavy-quark model under an external magnetic field shares the following qualitative similarities with the light-quark model:

- At fixed temperature T and chemical potential μ , the magnetic field suppresses the running coupling constant α .

- The running coupling α decreases monotonically with increasing energy scale E (at fixed T and μ), consistent with asymptotic freedom. This trend remains robust even in magnetized systems.
- In the QGP phase for light or heavy quarks model, α demonstrates pronounced sensitivity to T and μ , regardless of anisotropy ($c_B = 0$ or $c_B \neq 0$).

A promising direction for future research would be to systematically investigate how magnetic fields modify the holographic beta function in holographic QCD frameworks, particularly in comparison to the zero-field case considered in [18].

Acknowledgments

We thank K. Runnu and M. Usova for their valuable discussions.

The work of I. A., P. S. and A.N. is supported by Theoretical Physics and Mathematics Advancement Foundation “BASIS” (grant No. 24-1-1-82-1, grant No. 23-1-4-43-1 and grant No. 24-2-2-4-1, respectively). The work of A. H. was performed at the Steklov International Mathematical Center and supported by the Ministry of Science and Higher Education of the Russian Federation (Agreement No. 075-15-2022-265).

References

- [1] I. Y. Aref'eva, A. Hajilou, A. Nikolaev and P. Slepov, "Holographic QCD running coupling for light quarks in strong magnetic field," *Phys. Rev. D* **110** no.8, 086021 (2024) [arXiv:2407.11924 [hep-th]]
- [2] I. Y. Aref'eva, A. Hajilou, P. Slepov and M. Usova, "Running coupling for holographic QCD with heavy and light quarks: Isotropic case," *Phys. Rev. D* **110**, no.12, 126009 (2024) [arXiv:2402.14512 [hep-th]].
- [3] S. Navas *et al.* [Particle Data Group], "Review of particle physics," *Phys. Rev. D* **110**, no.3, 030001 (2024).
- [4] J. M. Maldacena, "The Large N limit of superconformal field theories and supergravity," *Adv. Theor. Math. Phys.* **2**, 231-252 (1998). [arXiv:hep-th/9711200 [hep-th]].
- [5] J. Casalderrey-Solana, H. Liu, D. Mateos, K. Rajagopal and U. A. Wiedemann, "Gauge/String Duality, Hot QCD and Heavy Ion Collisions", (Cambridge University Press, Cambridge, UK, 2014), [arXiv:1101.0618 [hep-th]].
- [6] I. Y. Aref'eva, "Holographic approach to quark-gluon plasma in heavy ion collisions", *Phys. Usp.* **57**, 527-555 (2014).
- [7] O. DeWolfe, S. S. Gubser, C. Rosen and D. Teaney, "Heavy ions and string theory", *Prog. Part. Nucl. Phys.* **75**, 86 (2014) [arXiv:1304.7794 [hep-th]].
- [8] O. Andreev and V. I. Zakharov, "Heavy-quark potentials and AdS/QCD," *Phys. Rev. D* **74** (2006), 025023 [arXiv:hep-ph/0604204 [hep-ph]].
- [9] I. Aref'eva and K. Rannu, "Holographic Anisotropic Background with Confinement-Deconfinement Phase Transition," *JHEP* **05**, 206 (2018) [arXiv:1802.05652 [hep-th]].
- [10] H. Bohra, D. Dudal, A. Hajilou and S. Mahapatra, "Anisotropic string tensions and inversely magnetic catalyzed deconfinement from a dynamical AdS/QCD model," *Phys. Lett. B* **801**, 135184 (2020) [arXiv:1907.01852 [hep-th]].
- [11] I. Y. Aref'eva, K. Rannu and P. Slepov, "Holographic model for heavy quarks in anisotropic hot dense QGP with external magnetic field," *JHEP* **07**, 161 (2021) [arXiv:2011.07023 [hep-th]].
- [12] I. Y. Aref'eva, A. Hajilou, K. Rannu and P. Slepov, "Magnetic catalysis in holographic model with two types of anisotropy for heavy quarks," *Eur. Phys. J. C* **83**, no.12, 1143 (2023) [arXiv:2305.06345 [hep-th]].
- [13] Y. Yang and P. H. Yuan, "Confinement-deconfinement phase transition for heavy quarks in a soft wall holographic QCD model," *JHEP* **12**, 161 (2015) [arXiv:1506.05930 [hep-th]].
- [14] B. Galow, E. Megias, J. Nian and H. J. Pirner, "Phenomenology of AdS/QCD and Its Gravity Dual," *Nucl. Phys. B* **834**, 330-362 (2010) [arXiv:0911.0627 [hep-ph]].

- [15] U. Gursoy and E. Kiritsis, “Exploring improved holographic theories for QCD: Part I,” *JHEP* **02**, 032 (2008) [arXiv:0707.1324 [hep-th]].
- [16] U. Gursoy, E. Kiritsis and F. Nitti, “Exploring improved holographic theories for QCD: Part II”, *JHEP* **02**, 019 (2008) [arXiv:0707.1349 [hep-th]].
- [17] H. J. Pirner and B. Galow, “Strong Equivalence of the AdS-Metric and the QCD Running Coupling”, *Phys. Lett. B* **679**, 51-55 (2009) [arXiv:0903.2701 [hep-ph]].
- [18] I. Y. Aref’eva, A. Hajilou, P. Slepov and M. Usova, “Beta-functions and RG flows for holographic QCD with heavy and light quarks: Isotropic case,” *Phys. Rev. D* **111**, no.4, 046013 (2025)
- [19] S. He, M. Huang and Q. S. Yan, “Logarithmic correction in the deformed AdS₅ model to produce the heavy quark potential and QCD beta function,” *Phys. Rev. D* **83**, 045034 (2011) [arXiv:1004.1880 [hep-ph]].
- [20] H. Bohra, D. Dudal, A. Hajilou and S. Mahapatra, “Chiral transition in the probe approximation from an Einstein-Maxwell-dilaton gravity model,” *Phys. Rev. D* **103**, no.8, 086021 (2021) [arXiv:2010.04578 [hep-th]].
- [21] M. W. Li, Y. Yang and P. H. Yuan, “Approaching Confinement Structure for Light Quarks in a Holographic Soft Wall QCD Model,” *Phys. Rev. D* **96**, no.6, 066013 (2017) [arXiv:1703.09184 [hep-th]].
- [22] X. Chen, L. Zhang, D. Li, D. Hou and M. Huang, “Gluodynamics and deconfinement phase transition under rotation from holography,” *JHEP* **07**, 132 (2021) [arXiv:2010.14478 [hep-ph]].
- [23] I. Y. Aref’eva, A. Ermakov, K. Rannu and P. Slepov, “Holographic model for light quarks in anisotropic hot dense QGP with external magnetic field,” *Eur. Phys. J. C* **83**, no.1, 79 (2023) [arXiv:2203.12539 [hep-th]].